

A spatial atlas of the complement system uncovers unique expression patterns in postnatal brain development in mice

Received: 31 August 2025

Accepted: 27 October 2025

Published online: 02 December 2025

 Check for updates

Yingying Zhang  ¹, Brianna Watson  ^{1,2}, Ajitanuj Rattan  ¹, Tyrone Lee  ³, Smriti Chawla ³, Ludwig Geistlinger ³, Yilin Guan ¹, Finley B. Lord ¹, Minghe Ma  ¹, Takashi Miwa ⁴, Madhu Golla  ⁴, Barbara J. Calderone ⁵, Wen-chao Song ⁴, Jeffrey R. Moffitt  ^{1,2}  & Michael C. Carroll  ^{1,6} 

Recent studies have found non-immunological roles of the classical complement pathway (CP) in brain development and its involvement in neuropsychiatric and neurodegenerative diseases. However, multiple complement activation pathways exist beyond the CP, but their expression and function remain poorly understood in the brain. Using MERFISH, we constructed a comprehensive spatial transcriptomic atlas of the complement system in mouse brains from late embryonic stage to adulthood. Here we show that most complement genes are expressed locally with a remarkable degree of cellular, spatial, and temporal heterogeneity and that complement regulatory mechanisms are distinct from the periphery. Beyond confirming the known expression of the CP, our measurements reveal endogenous expression of the alternative pathway (AP), notably the AP activator Masp3 in immature brains. Masp3 deficiency alters molecular structure of the brain and causes working spatial memory defects, indicating a role of Masp3 in brain maturation, potentially via modulation of AP activity.

The complement system is a well-characterized key regulator of both innate and adaptive immunity^{1,2} with over 50 known complement-related genes in rodents, consisting of complement cascade components, receptors, and regulators. The complement cascade can be activated through three distinct pathways: the classical pathway (CP), the lectin pathway (LP), and the alternative pathway (AP). Numerous studies have shown that the CP mediates microglia-dependent synapse pruning during normal neural development^{3–6}, and that its over-activation can cause Schizophrenia^{7–10}. Moreover, complement activation has also been frequently implicated in the progression of many neurodegenerative diseases^{11–18}. However, unlike in the periphery, our understanding of the complement system in the brain remains

incomplete. For example, the expression and regulation of the complement cascade in different brain regions, cell types, and across postnatal development stages have not been comprehensively determined. And, while the role of the CP in neuronal development is clear, it remains unknown if the LP and AP are involved in brain development, and if so, whether their functions are redundant with the CP.

As many of the complement genes are lowly and heterogeneously expressed in the brain, it is technically challenging to profile their expression by single-cell RNA sequencing, due to constraints in sequencing depth, transcript capture efficiency, and the number of cells profiled. Moreover, tissue dissociation for such characterization naturally disrupts the spatial context. The low and heterogeneous

¹Program in Cellular and Molecular Medicine, Boston Children's Hospital, Boston, MA, USA. ²Department of Microbiology, Blavatnik Institute, Harvard Medical School, Boston, MA, USA. ³Department of Biomedical Informatics, Core for Computational Biomedicine, Blavatnik Institute, Harvard Medical School, Boston, MA, USA. ⁴Department of Systems Pharmacology and Translational Therapeutics, Perelman School of Medicine, University of Pennsylvania, Philadelphia, PA, USA. ⁵Mouse Behavior Core, Harvard Medical School, Boston, MA, USA. ⁶Department of Pediatrics, Harvard Medical School, Boston, MA, USA.

 e-mail: Jeffrey.Moffitt@childrens.harvard.edu; Michael.Carroll@childrens.harvard.edu

expression also make it technically challenging to detect complement proteins by immunohistochemistry (IHC). Furthermore, as many complement components are secreted, IHC does not define the regional or cellular sources.

Multiplexed Error-Robust Fluorescent *in situ* Hybridization (MERFISH), a spatial transcriptomic method with single-cell resolution, has emerged as a potential solution to these challenges^{19–21}, with the demonstrated ability to profile hundreds to thousands of genes, including lowly expressed genes, and from these measurements define, discover, and map cell types in different regions of the mouse and human brain^{20,22–25}. Recently, MERFISH and related methods have been extended to define and map cell populations across the entire adult mouse brains^{25–27}. By then integrating these measurements with companion single-cell RNA sequencing datasets, the transcriptome-wide gene expression and spatial organization of thousands of neuronal populations have been described. However, only a very limited number of genes in the complement pathway were included in the target gene set in these studies. Thus, given the limited sensitivity of single-cell RNA sequencing, inferred complement gene expression through data integration remains low in resolution and accuracy. Moreover, these studies have been limited to adult mice, leaving the developmental regulation, a critical aspect of complement function in the brain, unexplored.

To address these limitations, we report here a comprehensive overview of the complement system in mouse brains from late embryonic stage (embryonic day 18.5/E18.5) to adulthood (postnatal day 120/p120) profiled with MERFISH. Our data showed that beyond the established expression of CP, most of the complement genes (47 out of 51 profiled) are locally expressed across different brain regions. Supporting the functional significance of this expression, we find that complement expression is differentially regulated by brain region and cell type and that these expression patterns evolve with age. Consistent with prior findings²⁸, our data support an induction of the CP over time. Extending beyond these observations, we find below threshold expression of essential LP serine protease gene *Masp2* along with ample expression of the LP inhibitor gene *Map44*, suggesting a limited local source for LP activation in healthy young brains. By contrast, AP genes are expressed in the brain, particularly in immature brains. Depletion of the AP activator *Masp3* shifts the distribution of subsets of cortical vGlut1⁺ excitatory neurons, and in parallel, results in spatial working memory defects. Collectively, these findings suggest a role of *Masp3* and, by extrapolation, the AP, in brain maturation.

Results

Complement components are locally produced in the brain with cell-type and brain-region heterogeneity

To construct a brain atlas for the complement system, we designed a 249-gene MERFISH probe library comprising genes in the following groups: (1) canonical markers for major brain cell types; (2) cortical layer and brain region markers; (3) neurotransmitter synthesis, transport and receptors; (4) known genes involved in neural development and homeostasis; and (5) 51 complement genes, including complement components, receptors and regulators (Table S1). Given the tremendous heterogeneity of cell types in the brain, and the lack of a consensus for terminal neuronal and glial cell types, our goal with this library was to determine complement expression in major categories of cells in the brain parenchyma. From six whole sagittal sections from postnatal day 60 (p60) young adult mouse brains, we decoded over 250 million RNA molecules that were assigned to over half a million segmented cells (Fig. 1). Overall, the measured gene expression was highly reproducible between replicates (Fig. S1A) and well correlated with published abundance values from bulk RNA-sequencing of the brain (Fig. S1B). In addition, the RNAs included to mark different brain regions detected by MERFISH showed expected spatial distribution

patterns that matched those from the Allen Brain Atlas (ABA) *in situ* hybridization database (Fig. S1C).

Using these measurements, we identified 16 major brain cell types based on established cell type markers (Figs. 1A, B, S1D, a full list of cell type abbreviations can be found in Table S2). We then performed a second round of clustering to refine cell types and place them in distinct brain regions (Figs. 1C–K, S2), resulting in 17 subtypes of vGlut1⁺ neurons, 12 subtypes of vGlut2⁺ neurons, and 12 subtypes of inhibitory neurons. vGlut1⁺ neurons mainly occupied the cortex and cerebellum, and their subclusters formed distinct cortical layers and sub-structures of the hippocampus (Figs. 1D, S2A, B). vGlut2⁺ neurons mainly located in the brain stem and segregated into various nuclei in the thalamus and mid-/hind-brain (Figs. 1E, S2C, D). Inhibitory neurons formed transcriptionally distinct subclusters in the cortex, striatum, mid-/hind-brain and the cerebellum. In the thalamus, inhibitory neurons were most densely located in the reticular nucleus (IN-RT) as expected^{29–31} (Figs. 1F, S2E, F). Similarly, subtypes of astrocytes (Figs. 1G, S2G, H) and oligodendrocytes (Figs. 1H, S2I, J) also segregated by brain regions, whereas microglia (Figs. 1I, S2K, L), oligodendrocyte progenitor cells (Figs. 1J, S2M, N), and endothelial cells (Figs. 1K, S2O, P) did not display brain-region specific sub-populations. We leveraged these spatial distribution properties to identify 23 distinct brain regions and assigned cells to these regions (Fig. 1C, a full list of brain region abbreviations can be found in Table S3).

We next evaluated the spatial and cell-type expression pattern of the complement genes. As false positive signals are present in image-based approaches to single-cell transcriptomics, such as MERFISH, we included eight barcodes that were not assigned to any target RNA in the library (termed “blanks”) to measure this false positive rate. Genes detected at least 2 standard deviations above the average of blanks in at least 1 cluster of cells were considered as expressed. 44 out of 51 (86.3%) complement genes examined were expressed above this threshold in at least one cluster (Figs. S3 and S4). *C1rb*, *Hc* (encoding *C5*), *C9*, *C4bp*, *Fcna*, *Masp2* and *Vsig4* did not pass this threshold in p60 mouse brains. Nonetheless, for completeness we report the observed average expression for these genes by major brain cell types (Fig. S3) and refined subclusters (Fig. S4). Figure 2A summarizes genes involved in different complement pathways and their overlap. We have constructed an interactive online platform to facilitate the visualization of these data (https://moffittlab.github.io/visualization/2024_Complement_Brain/index.html).

Genes in the CP were most highly expressed by glial cells in the brain (Fig. S3). Among them, the genes of the C1q pattern recognition complex (*C1qa*, *C1qb*, *C1qc*) were highly and exclusively expressed by microglia (MG) and perivascular macrophages (PVM) (Figs. 2B left panel, 2C, S3), with relatively homogeneous distribution across different brain regions (Fig. 2D, E), observations that are consistent with findings in published single-cell RNA sequencing studies in both human and mouse brains^{22–34}. CP activation requires serine proteases *C1r* (encoded by *C1ra* and *C1rb*) and *C1s* (encoded by *C1s1* and *C1s2*) downstream of the C1q complex. In contrast to genes encoding the C1q complex, *C1r/s* genes were sparsely expressed only in a few cell types and in restricted brain regions—mainly cells of the choroid plexus (ChP) and pericytes (Figs. 2B, middle and right panels, 2C–E, S3)—suggesting these essential components for CP activation could be made available through circulating cerebral-spinal fluid (CSF) produced by the ChP and through paracrine secretion by pericytes that are found in the base membrane of capillaries. In addition, limited local expression of *C1r/s* genes may be a mechanism to prevent complement overactivation at steady state.

LP components were generally very sparsely expressed in the brain (Fig. 2F–I), mainly by small subsets of neurons. Among the LP components, pattern recognition molecules *Fcnb*, *Mbl1*, and *Mbl2* were detected above background (Figs. 2F, left and middle panel, 2G, S3). Spatially, they were enriched in the cortex and the ChP (Fig. 2H). Within

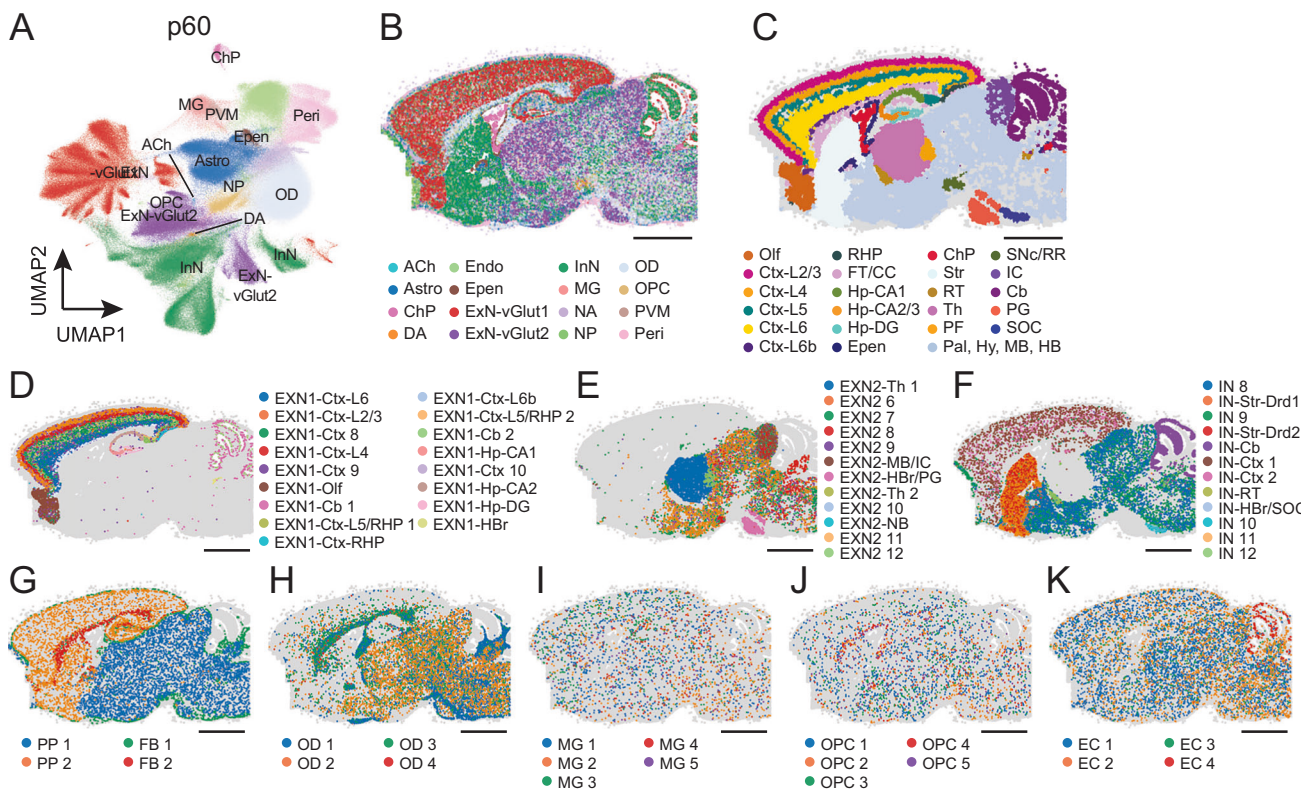


Fig. 1 | Cell type and brain region identification in young adult mouse brain by MERFISH. **A** UMAP visualization of primary cell clusters identified by MERFISH in p60 mouse brain sagittal sections. **B** The spatial localization of each primary cell type in a representative brain slice. Cells are colored by cell type as in (A). **C** The spatial location of identified brain regions for the slice in (B). Spatial localization of secondary cell clusters of vGlut1* (ExN-vGlut1, **D**) and vGlut2* (ExN-vGlut2, **E**) excitatory neurons, inhibitory neurons (InN, **F**), astrocytes (Astro, **G**),

oligodendrocytes (OD, **H**), microglia (MG, **I**), oligodendrocyte progenitor cells (OPC, **J**) and endothelial cells (Endo, **K**) for the slice in (B). Full lists of cell type and brain region abbreviations can be found in Tables S2 and S3, respectively. Note that PF (parafascicular region) and RT (reticular nucleus) are thalamic nuclei, and that Th designates other thalamic regions that are not further distinguished. Scale bar: 2 mm. Source data are deposited on Data Dryad (<https://doi.org/10.5061/dryad.cnp5hqcba>).

the cortex, *Fcnb* was enriched in superficial cortical layers 2-4, but *Mbl1* and *Mbl2* were enriched in deep cortical layers 5 and 6 (Fig. 2I). However, the level of *Masp2*, which encodes the serine protease essential for LP activation, was below detection limit in all cell types, suggesting a minimal local source of LP in healthy young adult mouse brains.

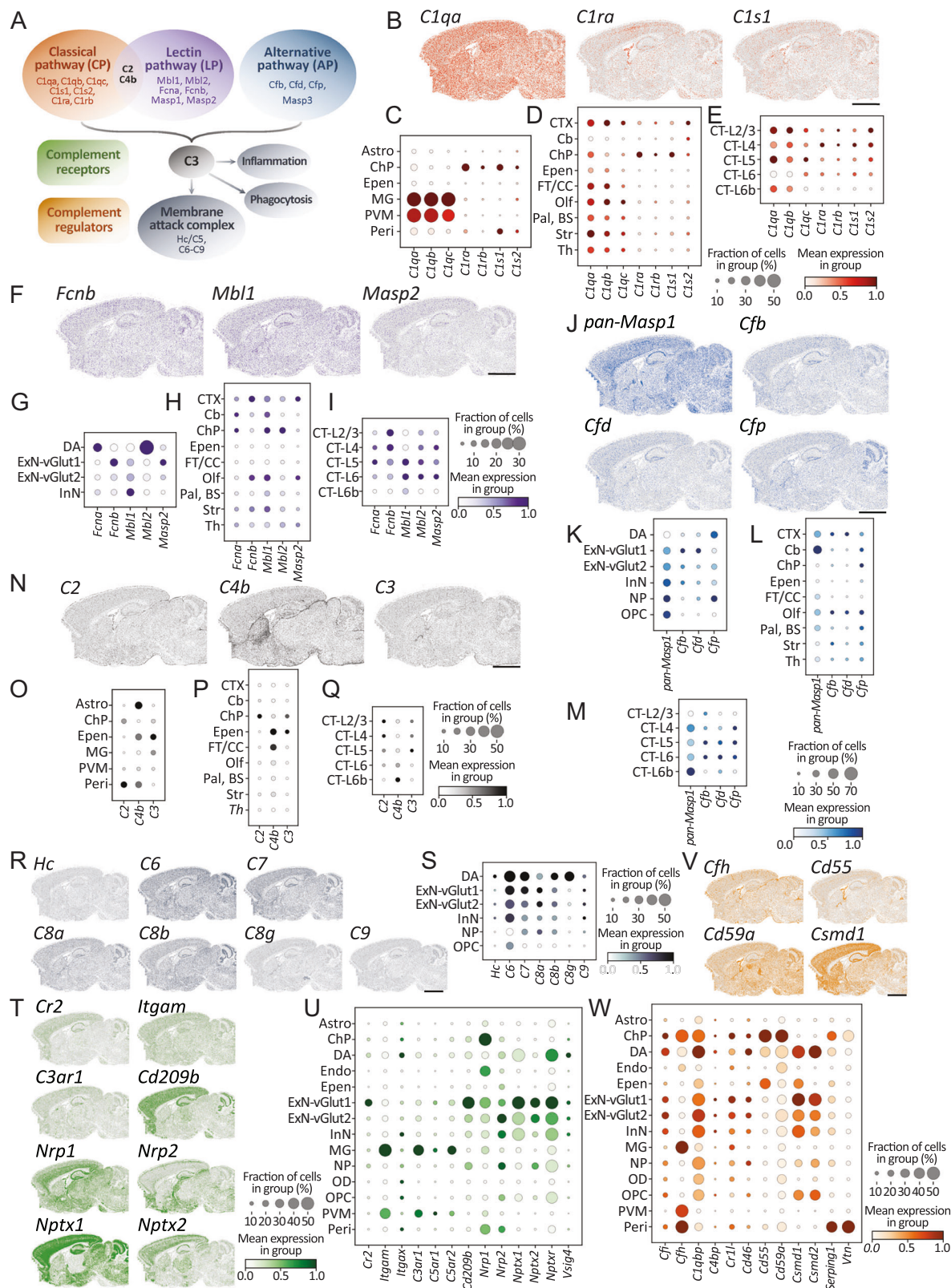
The AP does not involve pattern recognition factors but requires complement factor B (Cfb) and factor D (Cfd), and is positively regulated by properdin (Cfp)³⁵ and the serine protease Masp3³⁶. *Masp3* is a distinct transcript variant encoded by the *Masp1* gene. And due to high sequence similarity among the isoforms, MERFISH probes for the *Masp1* gene were not designed to distinguish its isoforms. We therefore refer to the *Masp1* gene as *pan-Masp1* to distinguish the gene from the transcript variants and to indicate isoform non-specific detection with MERFISH. Transcripts of all AP components were detected above threshold, particularly in various types of neurons, neural and oligodendrocyte progenitor cells (Figs. 2J, K, S3). Besides the cerebellum and the olfactory area, their expression was also enriched in the cortex (Fig. 2L), especially in deep cortical layers five and six (Fig. 2M). These observations indicate a previously unappreciated presence of the AP in the brain. Notably, AP activator *Cfp* was mostly highly expressed by neural progenitor cells (Fig. 2K), further suggesting a role of the AP in these cells.

Both CP and LP activate C2 and C4b, and then converge with the AP and activate C3. C2, C4b and C3 transcripts were all detected above threshold but sparsely distributed in the brain (Fig. 2N). They were mainly detected in glial cells, with C2 expressed by pericytes and the ChP, C4b by astrocytes (notably Gfap⁺ fibrous astrocytes, Fig. S4D),

ependymal cells and pericytes, and C3 by microglia (Figs. 2O, S3). Spatially, C2, C4b and C3 were enriched in structures surrounding the brain ventricles, including the fiber tract and corpus callosum, the ChP, and the ependyma, and showed generally low expression levels in other brain regions (Fig. 2P, Q). These observations suggest a unique aspect of complement regulation in the brain. Unlike in the periphery where C4b and C3 are among the most abundant serum proteins, the brain has very limited access to these components at homeostasis, either from a local source or from the serum due to the blood-brain barrier. Such restricted levels may represent a mechanism to prevent damage from complement overactivation.

Complement activation eventually results in the formation of the membrane attack complex, a plasma membrane pore composed of C5-C9, which can trigger inflammatory response and lead to catastrophic lytic cell death³⁷. This process is therefore tightly regulated. In the brain, transcripts of C6, C7 and all three subunits of C8 (C8a, C8b, C8g) were detected above threshold (Figs. 2R, S, S3). However, the local expression of two essential components of MAC, C5 (encoded by *Hc*) that initiates MAC formation, and the pore-forming subunit C9, was below threshold, suggesting transcriptional level suppression of MAC in healthy young brains. We further speculate that local expression of C6-C8 could indicate the “preparedness” of the brain to respond to inflammatory and disease conditions. To support this idea, dysregulated MAC formation has been implicated in the pathogenesis of Alzheimer’s disease in mouse models^{38,39}.

Complement receptors are additional essential components in the cascade. Based on their cell type expression patterns, we loosely grouped the complement receptors into two categories: those



expressed by microglia, cell types that respond to complement activation through receptor-ligand binding, and those expressed by neurons (Fig. 2T, U, S3). Microglia function as brain tissue resident macrophages, and similar to their peripheral counterparts, they expressed *Itgam* (encoding Cd11b/Cr3), the receptor for complement iC3b, that allows microglial phagocytosis of complement opsonized synapses in development and diseases. In addition, microglia were also

the main cell type that expressed *C3ar1*, *C5ar1* and *C5ar2*, encoding receptors for anaphylatoxins C3a and C5a produced upon complement activation. *C5ar1* is known to drive pro-inflammatory response, whereas *C5ar2* has been reported to sequester C5a and have immunomodulatory functions⁴⁰. In the brain, *C5ar2* expression is significantly higher than that of *C5ar1*, suggesting a way in which inflammation may be regulated in healthy young brains.

Fig. 2 | Complement expression in p60 young adult mouse brains. **A** A simplified summary of complement component genes, their involvement in complement activation pathways, and genes that are shared across different complement pathways. Genes of complement receptors and regulators are not enumerated. **B** Representative plots of the spatial distribution of transcripts detected by MER-FISH of selected CP-specific genes (*C1qa*, *C1ra* and *C1s1*). These genes were selected to highlight the heterogeneity in overall abundance and spatial distribution pattern. **C** Dot plots showing CP-specific gene expression pattern by cell type. Only top cell types that express these genes were plotted to facilitate visualization. Gene expression among all major brain cell types can be found in Fig. S3. Dot plots

showing CP-specific gene expression pattern by broad brain regions (**D**) and by cortical layers (**E**). **F–Q** Similar plots as in (**B–E**) for LP-specific (**F–I**), AP-specific (**J–M**) and genes involved in at least two complement activation pathways (**N–Q**). **R** Spatial distribution of transcripts of genes to form the MAC. **S** Dot plots showing cell type expression pattern of MAC genes. Similar plots as in (**R, S**) for complement receptor genes (**T, U**) and complement regulatory genes (**V, W**). Full lists of cell type and brain region abbreviations can be found in Tables S2 and S3, respectively. Scale bar: 2 mm. Source data are deposited on Data Dryad (<https://doi.org/10.5061/dryad.cn5hqc6q>).

Neurons, especially vGlut1⁺ excitatory neurons, expressed abundant level of receptors to C1q, including *Cd209b* (encoding DC-SIGN, mouse homologue to SIGN-R1), and neuronal pentraxins *Nptx1*, *Nptx2*, and *Nptx3*^{41,42} (Figs. 2T, U, S3), which may serve as a docking site for C1q and downstream complement deposition. *Nrp1*, a newly identified receptor for complement split products⁴³, was expressed by neurons, ChP, endothelial cells and pericytes in addition to microglia (Figs. 2U, S3), reflecting its previously established function neuronal and vascular systems through interaction with semaphorins and VEGF^{44,45}.

The complement cascade is tightly regulated by complement regulators at almost every stage of its activation. At the level of complement initiation, *Serpinc1*, which inhibits both CP and LP serine proteases⁴⁶, was highly expressed by the pericytes and the ChP (Figs. 2W, S3). To regulate further complement activation at the level of C4b and C3, membrane-bound regulator *Csmd1*^{47–49}, and its structural homolog *Csmd2*, were highly expressed by neurons, neural progenitor and oligodendrocyte progenitor cells (Figs. 2V, W, S3). Factor I (*Cfi*) that proteolytically inactivates C3, and its cofactors C4 binding protein (*C4bp*) and membrane cofactor protein (MCP, encoded by *Cd46*) were detected at low levels in many brain cell types, notably neurons (Figs. 2W, S3). Complement factor H (*Cfh*), a soluble regulator that limits the amount of active C3 and C5 convertases from the alternative pathway, was highly expressed in microglia, pericytes and the ChP. Decay-accelerating factor (DAF, encoded by *Cd55*), a membrane-bound C3 convertase inhibitor, was highly expressed in the choroid plexus and ependyma (Figs. 2V, W, S3). Finally, membrane attack complex formation is under the control of soluble complement S-protein vitronectin (*Vtn*) and clusterin (*Clu*)^{50,51}, and membrane-bound regulator *Cd59* (encoding the MAC inhibitory protein)⁵². *Vtn* was mostly expressed by pericytes, whereas *Cd59* was most highly expressed by the ChP, but was also broadly detected in neurons (Figs. 2V, W, S3). *Clu* was not included in our library due to very high expression level reported in previously published mouse brain bulk RNA sequencing experiments.

Collectively, we showed that the vast majority of the complement genes profiled are locally expressed in the brain. Their expression patterns vary in overall abundance, cell-type and regional distributions. In addition to confirming previously known expression of CP genes in the brain, our data suggest an insufficient brain-endogenous expression of LP genes, but sufficient local expression of AP genes to support their activation. Furthermore, through both the protection of blood-brain barrier and low local gene expression, the brain is exposed to limited levels of essential components for complement activation, such as serine proteases, C3 and C4, and MAC components C5 and C9. Finally, each stage of complement activation is tightly regulated through the expression of conventional and brain-enriched complement regulators in various cell types. These observations suggest that complement expression is tuned to ensure controlled activity in the brain at steady state, yet allow the brain to respond rapidly and efficiently to infection or disease conditions.

Complement expression is developmentally regulated

It is well established that postnatal synaptic pruning^{3–6}, a highly dynamic process that happens at different ages depending on the

brain region, is driven in part by the CP. Moreover, the expression of complement components important for synaptic pruning, such as C1q, is dynamically regulated over development and normal aging²⁸. Given this role for complement in brain development, we asked if the expression pattern of other complement genes may also change over age. We therefore expanded our MERFISH measurement to the brains from late gestation stage embryos at embryonic day 18.5 (E18.5, n = 4), neonates at postnatal day 5 (p5, n = 6), and 4-month-old mature adults (p120, n = 3). As above, we identified all expected major cell clusters and assigned brain regions in samples across age groups (Fig. S5). Supporting our measurements, expression of neurogenesis and proliferation markers such as *Mki67*, *Dcx*, *Sox4*, *Sox11*, and *Cd24a*, declined over age (Fig. S5F) while the mature oligodendrocyte marker *Opalin*, and several neural transmission genes, including *Slc17a7* (encoding vGlut1), glutamate receptors *Grin2a*, *Grin2c* and GABA receptor type A subunit *Gabrd* (Fig. S5F) were enriched in adult brains.

Across all age groups measured, 47 out of 51 (92.2%) complement genes examined in MERFISH were expressed above background in at least one age group. Only *C1rb*, *Hc*, *C4bp* and *Masp2* showed no above background expression at any age. This observation further supports the notion that while most complement components are expressed locally over time, the brain prevents complement overactivation by limiting expression of key regulators such as *Masp2* and *Hc*. Furthermore, cell type-specific complement gene expression patterns remained consistent over time (Fig. S6), suggesting that these expression patterns are cell type intrinsic. However, clear changes were observed in both the overall abundance (Fig. 3A–D) and spatial distribution (Fig. S7) of many complement genes, indicating developmental regulation of complement expression.

We next explored each complement pathway in more depth. CP genes were generally much more abundant in adult brains compared to embryonic and juvenile brains, including the genes encoding the C1q/r/s complex, as well as C2, C4b and C3 (Fig. 3A). An increase in *C1qa* is the result of a combination of increased microglia abundance and increased cellular expression by microglia (Fig. 3E). In contrast, expression of *C1qb* and *C1qc* per microglia declined over time (Fig. 3E, top panel), and therefore the overall increase in *C1qb* and *C1qc* abundance is predominantly a result of microglia expansion. In addition, neuronal C1q receptor *Nptx1* was the top-enriched complement gene over time (Fig. 3C), further supporting a general induction of the potential to activate CP over development. Although expression of LP genes was induced at p120 (Fig. 3A), the *Masp2* expression level remained below threshold, suggesting insufficient local expression to support LP activation in all age groups tested. In contrast, multiple AP components, including *pan-Masp1*, *Cfd* and *Cfp*, were highly expressed in embryonic and juvenile brains (Fig. 3A). In parallel, expression of complement factor H (*Cfh*), an AP inhibitor, increased over time (Fig. 3D). Such transcription pattern suggests that if AP were active in healthy brains, it would be primarily in immature brains. As for MAC components, their expression was generally lower in p5 and p60 brains (Fig. 3B). Coincidentally, both MAC inhibitors *Cd55* (decay accelerating factor DAF) and *Cd59a* were enriched in p120 mature brains (Fig. 3D). These expression patterns of MAC components indicate that as the brain matures, it may have increased potential to activate the terminal

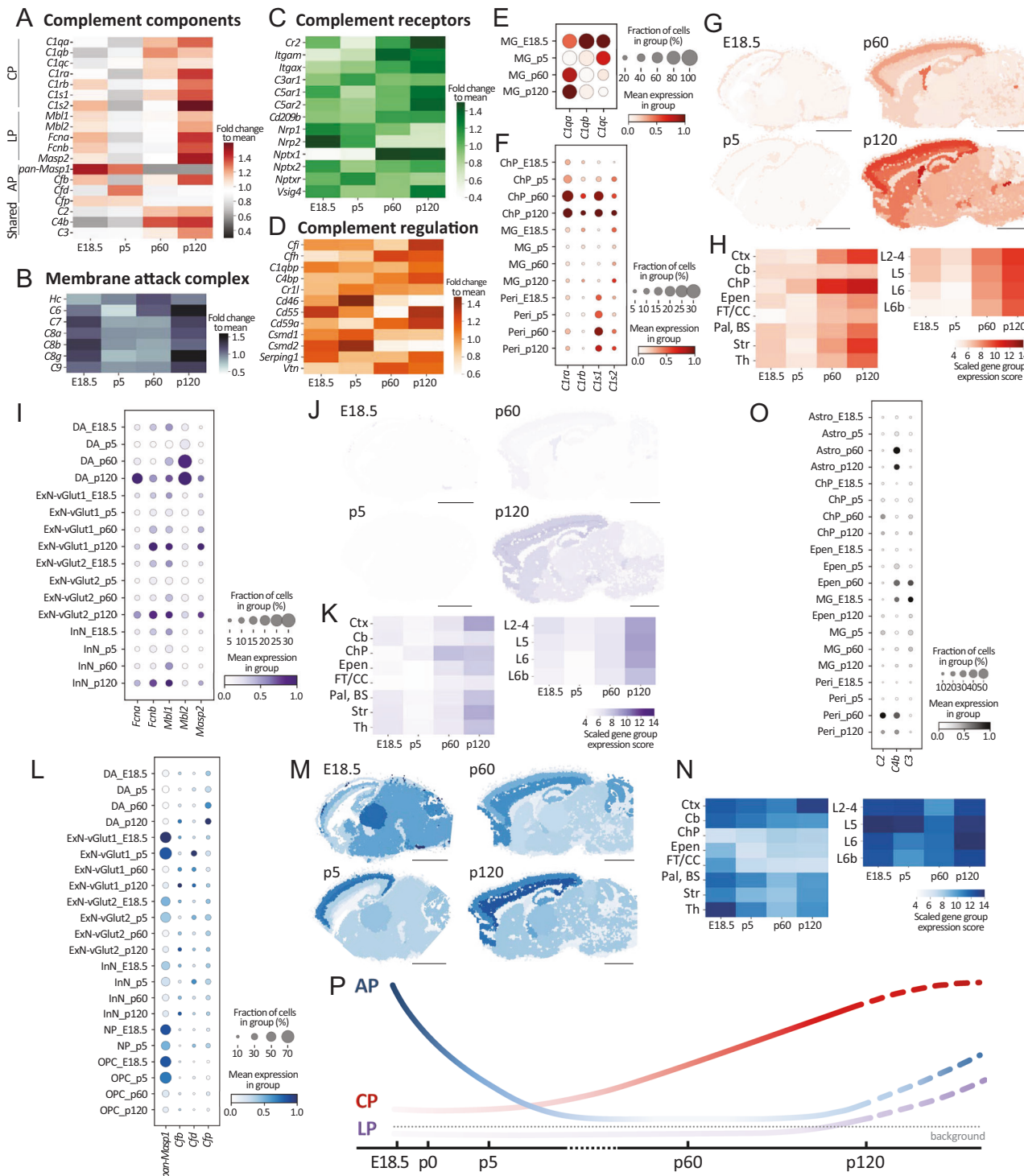


Fig. 3 | Developmental regulation of complement gene expression. Heatmap showing change of average expression over time from E18.5 to p120 of complement components involved in the three complement activation pathways (A), membrane attack complex (B), complement receptors (C) and regulatory genes (D). Average expression is calculated over all cells, regardless of their cell type and brain region, and normalized to the average of all age groups combined for each gene. Data is presented as fold change of the mean at a given age to the mean of all samples. E, F Dot plot showing change over time of expression in top expressing cell types for CP genes. G Representative spatial plotting of aggregated expression score of CP in E18.5, p5, p60 and p120 brains. The expression of *C1qa*, *C1qb*, *C1ra*, *C1rb*, *C1s1*, *C1s2*, *C2*, *C4b* and *C3* were included in the calculation. H Heatmap showing aggregated expression score of CP by broad brain region (left panel) and by cortical

layers (right panel) over age. Same genes as in (G) were included in the calculation. I-N Similar plots as in (E-H) for LP (I-K) and AP (L-N). The expression of *Mbl1*, *Mbl2*, *Fcnb*, *Masp1*, *C2*, *C4b* and *C3* were included in the calculation for LP; the expression of *pan-Masp1*, *Cfd*, *Cfb*, *Cfp* and *C3* was included for AP. O Dot plot showing change over time of expression of genes shared among all three complement pathways in top expressing cell types. P Summary of overall availability of components in each complement activation pathway from brain endogenous RNA expression over time. Gray dashed line represents background that is set based on detection threshold. Colored dashed lines represent trends by extrapolation, rather than actual result measured in this study. Full lists of cell type and brain region abbreviations can be found in Table S2 and S3, respectively. Scale bar: 2 mm. Source data are deposited on Data Dryad (<https://doi.org/10.5061/dryad.cnphqcbq>).

pathway, but at steady state, it can prevent MAC damage by expressing sufficient regulatory proteins accordingly.

As complement components typically work in concert with other members in the same pathway, functional inference cannot be drawn from the expression of a single complement gene. Therefore, to better describe the overall availability of essential components from local gene expression for complement activation, we computed an aggregated complement expression score by brain region, calculated as the geometric mean of the expression of the genes involved in each complement activation pathway. For each pathway, pathway-specific initiation genes and relevant shared components are included in the calculation. As our data did not distinguish cortical layers 2/3 and cortical layer 4 in E18.5 brains, we combined cortical layers 2–4 for consistency among age groups.

This analysis showed that the overall expression of CP genes generally increased across all brain regions over time, with the highest expression score seen in the ChP, followed by the cortex. And within the cortex, the CP score gradually declined from superficial layers 2–4 to deep layers 6 and 6b (Fig. 3E, H). In addition, this analysis revealed an induction of LP gene expression in mature adult brain at p120, particularly in the cortex and striatum (Fig. 3I–K). However, sub-threshold levels of *Masp2* expression continued to suggest that if there is activation of LP in the brain, it is likely provided by peripheral sources of *Masp2* or, in the case of neuroinflammatory stimuli, driven by local induction of *Masp2* expression. As for AP, overall expression of its components was most enriched in E18.5 but showed brain-region-dependent regulation over age. Specifically, we observed a re-induction of AP expression in the p120 mature cortex, a trend that was much less pronounced in other brain regions (Fig. 3L–N). The change over time of the expression score of all three complement pathways is summarized in Fig. 3P. From these analyses, we observed that CP and AP genes expression patterns exhibited temporal and spatial (across cortical layers) complementarity, suggesting non-redundant function of these two pathways in brain development.

Alternative complement pathway activator *Masp3* is highly expressed in late embryonic brains

The unique cell-type and temporal regulation of *pan-Masp1* expression prompted us to focus on this gene. It is the only complement gene whose expression was most elevated in the embryonic brain and dramatically declined over time. It is also one out of two complement genes with ample expression in neuronal and oligodendrocyte progenitor cells, the other such gene being AP activator *Cfp*. These *pan-Masp1* expression patterns suggested a role in brain development and in progenitor cells during late embryonic stages to neonates.

Masp1 is a complex gene. It encodes three functionally distinct variants that are derived from alternative splicing: the serine protease *Masp1* that activates the LP; *Map44* that acts as a LP inhibitor; and the serine protease *Masp3* that activates AP in a *Cfd*-dependent manner^{36,53,54} (Fig. 4A). Thus, to compare the relative abundance of each *Masp1* isoforms, we designed isoform specific primers (Fig. 4A) and performed digital droplet PCR (ddPCR) on mouse brain cortex and control liver samples. In p60 brains, *Map44* was the most abundant isoform, followed in abundance by *Masp3*, while *Masp1* was below detection limit (Fig. 4B). By contrast, *Masp1* was the most abundant isoform in the liver (Fig. 4C), confirming our ability to detect this transcript and suggesting a brain-specific regulation of the relative abundance of these isoforms. Consistent with MERFISH observation (Fig. 3A), the expression of all *Masp1* isoforms declined over time (Fig. 4D–F), but their relative abundance did not change. The expression pattern of *Masp1* isoforms was further validated by RNAscope using *pan-Masp1* and isoform-specific probes in E18.5 and p120 frontal cortex (Fig. 4G).

Together, these results indicate that the *pan-Masp1* transcripts detected by MERFISH likely represent the expression of the *Masp3* and

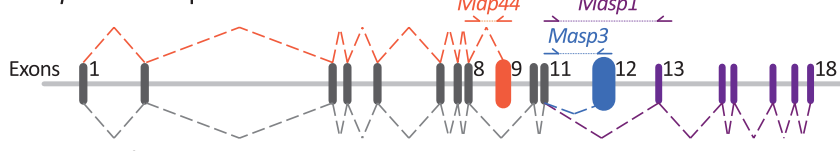
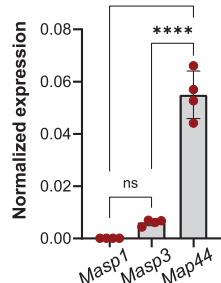
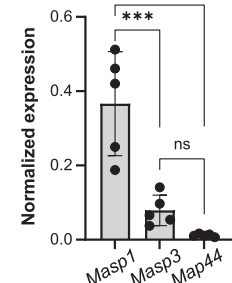
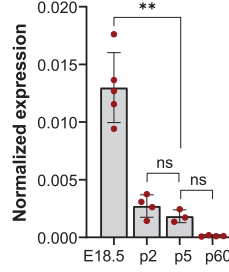
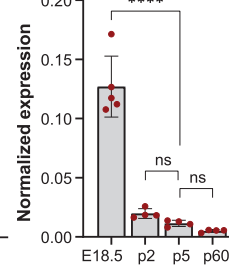
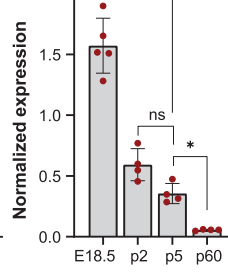
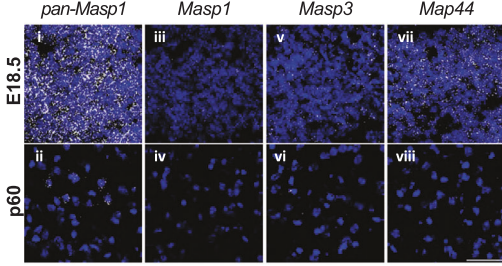
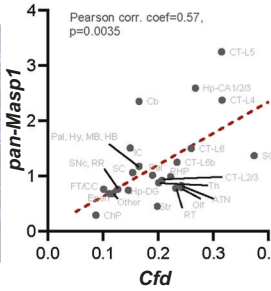
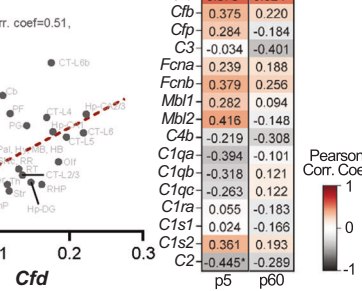
Map44 isoforms, but not the *Masp1* isoform in the brain. Below detection limit expression levels of *Masp1* and *Masp2*, together with ample expression of *Map44*, suggest LP inhibition in the brain. In contrast, expression of *Masp3* indicates possible AP activity in late embryonic to early postnatal brains.

To explore whether the *pan-Masp1* expression detected by MERFISH in the brain is consistent with the hypothesis of potential AP activity in the brain, we reasoned that for AP to be active, its components should be expressed in spatial proximity to the cells expressing *pan-Masp1*, especially *Cfd*, the direct downstream target of *Masp3*. As complement components mainly function as secreted factors, we further reasoned that regional co-expression may be more relevant than cell-type co-expression. To explore the regional covariation in complement expression, we calculated the average expression per brain region for complement genes that were detected above threshold by MERFISH. We first compared spatial expression patterns between *pan-Masp1* and *Cfd*, and, indeed, we found a strong positive correlation between them in both p5 (Fig. 4H, Pearson correlation coefficient=0.57, $p = 0.0035$) and p60 (Fig. 4I; Pearson correlation coefficient=0.51, $p = 0.01$) brains. To extend this analysis to other relevant complement component genes, we computed pair-wise Pearson correlation coefficient using their expression by brain region (Fig. 4J). We found that other AP genes, *Cfb* and *Cfp*, also shared some level of positive spatial expression correlation with *pan-Masp1* in p5 brains, a time point with relatively high *pan-Masp1* expression (Fig. 4J). Conversely, we noticed a significant negative correlation between *pan-Masp1* with *C2*, a gene shared between the CP and the LP, but not the AP (Fig. 4H), suggesting *pan-Masp1* expression is unlikely associated with CP and LP. In short, this correlation analysis supports that *pan-Masp1* expression may indicate brain AP activity.

Masp3 deficiency altered cortical distribution of vGlut1⁺ excitatory neuron subtypes in juvenile mice

To explore the *in vivo* function of *Masp3*, we turned to a *Masp3*-deficient mouse model⁵⁴. In this model, exon 12 of the *Masp1* gene was deleted via CRISPR/Cas9, which specifically inactivates the transcript variant encoding *Masp3*, leaving the other two transcript variants, which encode *Masp1* and *Map44*, respectively, intact⁵⁴. Indeed, a rabbit red blood cell hemolytic assay⁵⁴ showed that plasma AP activity was largely abrogated in *Masp3* homozygous knockout mice (*Masp3*^{−/−}) but not in heterozygous *Masp3* knockout mice (*Masp3*^{+/−}) or wild-type littermate controls (*Masp3*^{+/+}) (Fig. 5A), confirming AP attenuation in the *Masp3*^{−/−} mouse.

As *Masp3* is highly expressed in late embryonic and neonatal mouse brains, we performed MERFISH on p5 male *Masp3*^{+/+} and *Masp3*^{−/−} mouse brain sagittal sections. We again identified expected major brain cell types (Fig. 5B) and subclusters. Overall, our analyses did not indicate major cell type or gene expression changes caused by *Masp3* deficiency. However, we found that the loss of *Masp3* may affect the distribution and relative abundance of vGlut1⁺ excitatory neuron subclusters, specifically, subclusters 1 (sub-C1) and 6 (sub-C6; Fig. 5C, D). Spatially, sub-C6 occupied superficial cortical layers and overlapped with sub-C1 (Fig. 5E, orange: sub-C1; purple: sub-C6). In *Masp3*^{+/+} brains, sub-C6 cells spread throughout the anterior-posterior axis (Fig. 5E, left panel), whereas sub-C6 cells in the *Masp3*^{−/−} cortex (Fig. 5E, right panel) were restricted to the anterior cortex. Many of the top sub-C6 enriched genes (Fig. 5F) were those that increase in adult vGlut1⁺ neurons compared to juvenile neurons (Fig. 5G), including *Rbfox3* (encoding NeuN) and *Slc17a7* that are usually associated with mature neurons. Using RNAscope, we detected reduced expression of *Slc17a7* in the superficial layers of the posterior cortex of *Masp3*^{−/−} mice (Fig. 5H, I), consistent with MERFISH result that indicated a reduction of *Slc17a7*-high neurons in the same cortical area (Fig. 5E, F). In addition, sub-C6 neurons also expressed higher levels of neurotransmission genes that are most enriched in p5 vGlut1⁺ neurons compared to

A Masp1 transcript variants**B** *Masp1* isoform abundance in adult brain**C** *Masp1* isoform abundance in adult liver**D** *Masp1***E** *Masp3***F** *Map44***G****H****I****J****Fig. 4 | Masp3 expression is developmentally regulated in the brain.**

A Schematic drawing of the *Masp1* gene and alternative splicing of its transcript variants. Exons 1-8, and 10-11 (in gray) encode the regulatory domain found in both *Masp1* and *Masp3*. Serine protease domain of *Masp1* is encoded by exons 13-18 (in purple). *Masp1*-specific PCR primers amplify a sequence encoded by exons 11 and 13 (purple arrows). Exon 12 (in blue) encodes *Masp3*-specific serine protease domain. *Masp3*-specific PCR primers amplify a sequence encoded by exons 11 and 12 (blue arrows). *Map44* lacks the serine protease domain and is encoded by exons 1-9, with exon 9 (in orange) unique to the *Map44* transcripts. *Map44* specific PCR primers amplify a sequence encoded by exons 8 and 9 (orange arrows). Expression of *Masp1*, *Masp3* and *Map44* in p60 brain cortex (B) and liver (C) by ddPCR. n = 4 mice per age group; gender balanced. One-way ANOVA with Tukey's multiple comparisons test. In the cortex (B): *Masp1*: $8.8 \times 10^{-5} \pm 2.4 \times 10^{-5}$; *Masp3*: 0.0061 ± 0.0012 ; *Map44*: 0.0550 ± 0.0091 ; in the liver (C): *Masp1*: 0.3662 ± 0.1400 ; *Masp3*: 0.0791 ± 0.0411 ; *Map44*: 0.0119 ± 0.0038 . Expression of *Masp1* (D), *Masp3* (E) and *Map44* (F) over time by ddPCR. n = 5 mice for E18.5, n = 4 mice for all other age groups unless otherwise specified; gender balanced. One-way ANOVA with Tukey's multiple comparison test. For *Masp1* (D): E18.5: 0.0130 ± 0.0030 ; p2:

0.0007 ± 0.0010 ; p5: 0.0018 ± 0.0006 (n = 3); p60: $1.19 \times 10^{-4} \pm 0.49 \times 10^{-4}$; For *Masp3* (E): E18.5: 0.1270 ± 0.0258 ; p2: 0.0198 ± 0.0041 ; p5: 0.0115 ± 0.0026 ; p60: 0.0050 ± 0.0011 ; For *Map44* (F): E18.5: 1.572 ± 0.226 ; p2: 0.5927 ± 0.1316 ; p5: 0.3555 ± 0.0826 (n = 3); p60: 0.0555 ± 0.0051 . G Representative RNAscope image of pan-*Masp1* (isoform non-specific, i, ii), *Masp1* (iii, iv), *Masp3* (v, vi) and *Map44* (vii, viii) in the frontal cortex of E18.5 (top row) and p120 (bottom row) mice. Repeated in n = 3 mice per age group, images from one sample are shown. Scale bar: 50 μ m. Scatter plot of average normalized counts per cell of *Cfd* versus that of pan-*Masp1* by brain region detected by MERFISH in p5 (H) and p60 (I) brains. Each dot represents one brain region. A full list of brain region abbreviations can be found in Table S3. Pearson correlation test, two-tailed. Pearson correlation coefficient $r = 0.57$ in p5, $p = 0.0035$; $r = 0.51$ in p60, $p = 0.01$. J Heatmap of pair-wise two-tailed Pearson correlation coefficient of pan-*Masp1* expression by brain region with other complement components as detected by MERFISH in p5 (left column) and p60 (right column) samples. Complement components below detection threshold in all age groups are excluded. Pearson correlation coefficient is labeled on the heatmap. Error bars represent standard deviation; ns not significant; * $p < 0.05$, ** $p < 0.01$, *** $p < 0.001$, **** $p < 0.0001$. Source data are provided as a Source Data File.

other ages, such as glutamate metabotropic receptors *Grm3*, *Grm7*, and GABA receptor subunits *Gabra5*, *Gabrb3* (Fig. 5G). Differentially expressed genes between sub-C1 and sub-C6 suggest these cells may be at distinct maturation states. An alteration of the relative abundance of these neuronal subtypes indicates a role of *Masp3* in the neuronal maturation process, and a disruption in this process may further affect neuronal circuitry development. As neuronal maturation takes place over time and varies by brain region, further analysis at additional time points is necessary to determine whether *Masp3* only affects these two cortical excitatory neuron subtypes or has a broader impact.

Masp3 deficiency affected systemic development and caused spatial working memory deficits

Given the molecular changes observed in *Masp3*-deficient mouse brains, we speculated that these mice might have additional

neurological defects. We noted several broad physiological effects in the *Masp3*^{-/-} mice. These mice had a lower-than-expected birth rate: 20 out of 173 (11.6%, compared to expected 25% or 43 mice) female mice, and 23 out of 160 male mice (14.4%, compared to expected 25% or 40 mice) born from heterozygous breeding pairs were *Masp3*^{-/-} (Table S4). Among those that survived, *Masp3*^{-/-} mice had sustained lower body weight. On average, male *Masp3*^{-/-} weighed 20% less than littermate control *Masp3*^{+/+} males, and females weighed 14.5% less (Fig. 6A), indicating an important role of *Masp3* in systemic development.

To then explore neurological defects induced by the loss of *Masp3*, we tested cognition, motor function, anxiety and depression with a series of behavioral assays. A novelty Y maze test for spatial working memory was applied to assess cognitive function (illustrated in Fig. 6B). Both *Masp3*^{+/+} (n = 8, males, Fig. 6C, left panel) and *Masp3*^{-/-}

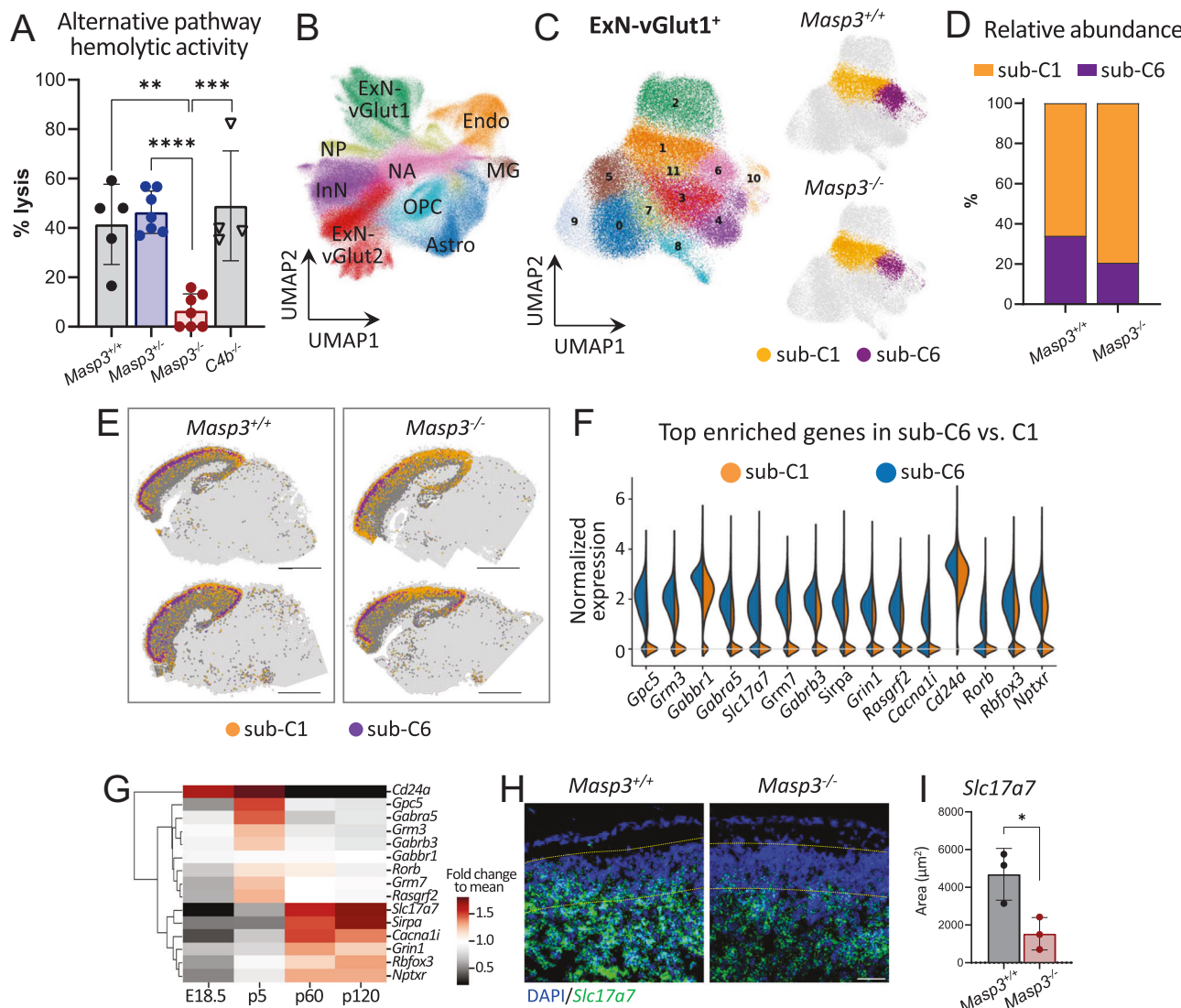


Fig. 5 | Masp3 deficiency affects cortical distribution of vGlut1+ excitatory neuron subtypes in early postnatal brains. **A** Rabbit red blood cell hemolytic assay with plasma from *Masp3*^{+/+} (n = 5 mice, 41.48% ± 16.25%), *Masp3*^{-/-} (n = 7 mice, 46.37% ± 8.55%), *Masp3*^{-/-} (n = 7 mice, 6.47% ± 6.80%) and *C4b*^{-/-} (n = 4 mice 48.95% ± 22.24%) mice. Percent hemolysis was reported by considering hemolysis in water as 100%. One-way ANOVA followed by Tukey's test for multiple comparison. Mixed gender. UMAP showing identification of major brain cell types (**B**) and vGlut1⁺ excitatory neuron sub-types by MERFISH in p5 *Masp3*^{+/+} and *Masp3*^{-/-} (**C**, left panel: all samples combined; right panel: separated by genotype with sub-C1 and sub-C6 highlighted). A full list of cell type abbreviations can be found in Table S2. **D** Stacked bar plot showing relative abundance of sub-C1 and sub-C6 of vGlut1⁺ excitatory neuron in *Masp3*^{+/+} and *Masp3*^{-/-} brains. **E** Spatial plotting of sub clusters 1 (orange)

and 6 (purple) of vGlut1⁺ excitatory neurons (dark gray) in *Masp3*^{+/+} (left) and *Masp3*^{-/-} (right) brain sagittal slices. Scale bar: 2 mm. **F** Violin plot showing expression of top enriched genes in sub-cluster 6 (blue) versus. sub-cluster 1 (orange). **G** Change over time of top differentially expressed genes between sub-C6 and sub-C1. **H** Representative images of *Slc17a7* (green) RNAscope in the posterior cortex of a p5 *Masp3*^{+/+} (left) and *Masp3*^{-/-} (right) mice. Scale bar: 100 μ m. **I** *Slc17a7* expression detected by RNAscope in superficial layers of the posterior cortex (excluding layer 1), quantified as *Slc17a7* signal area normalized to DAPI nuclei area. n = 3 mice per genotype. Unpaired t test, two tailed. *Masp3*^{+/+}: 4690 ± 1372; *Masp3*^{-/-}: 1539 ± 861. All male mice in (**B**–**I**). Error bars represent standard deviation; *p < 0.05, **p < 0.01, ***p < 0.001, ****p < 0.0001. Source data are provided as a Source Data File.

mice (n = 9, males, Fig. 6C, middle panel) showed expected preference for previously unexplored territory, as measured by time spent (Fig. 6D) and distance run (Fig. 6E) in the novel vs. familiar arms. However, the *Masp3*^{-/-} mice lack such preference (n = 7, males, Fig. 6C, right panel; Fig. 6D, E), indicating deficits in spatial working memory. We did not observe defects in other behavioral assays (Fig. S8), indicating that the loss of Masp3 did not affect motor function (Fig. S8A–B), induce anxiety (Fig. S8C), or cause depression (Fig. S8D–E). Thus, our results are consistent with a focused rather than broad role of Masp3 in the healthy development and function of the central nervous system. Nonetheless, we note that given the broad physiological effects introduced by Masp3 deficiency and the potential

for systemic effects, it is possible that these neurological effects do not reflect a direct effect of Masp3 on neurodevelopment.

Discussion

Here we used MERFISH to produce a spatially resolved brain atlas of the complement system over development. With our approach, we found that the brain has a local supply of most complement components, whose expression exhibited temporal, cellular and spatial heterogeneity. Complement activation in the brain is strictly regulated, with aspects that are distinct from the periphery. First, expression of serine proteases that are indispensable for complement cascade is maintained at very low level at steady state to keep minimal basal level

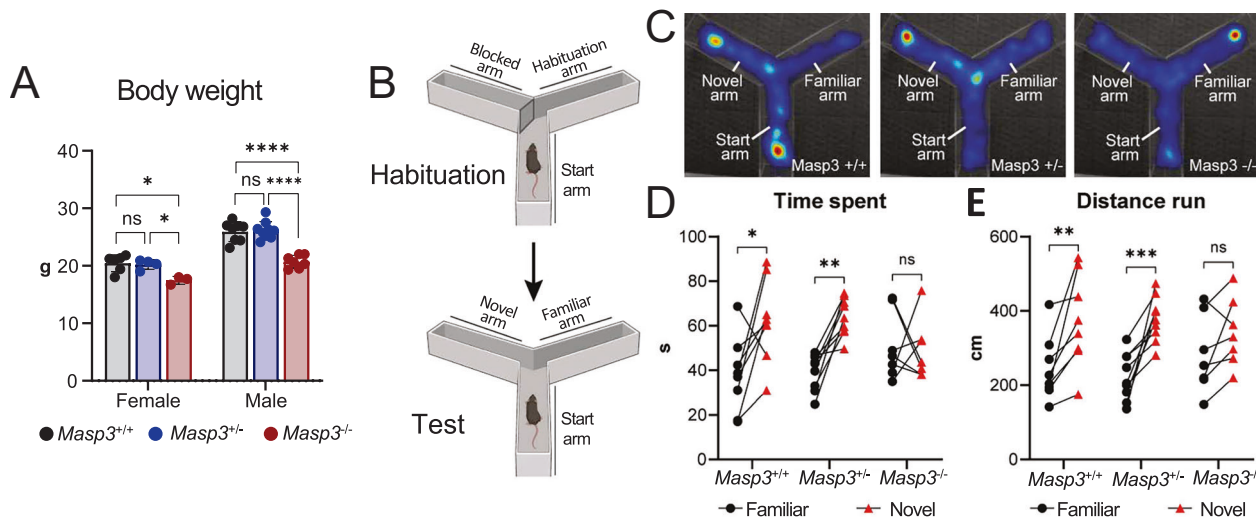


Fig. 6 | Masp3 deficiency resulted in spatial working memory deficits. **A** Body weight of 13–14-week-old adult *Masp3*^{+/+} (n = 6 females, 20.45 g ± 1.45 g; n = 8 males, 25.93 g ± 1.72 g), *Masp3*^{+/-} (n = 4 females, 20.23 g ± 0.85 g; n = 9 males, 26.17 g ± 1.53 g) and *Masp3*^{-/-} (n = 3 females, 17.47 g ± 0.68 g; n = 7 males, 20.71 g ± 1.10 g) mice. Two-way ANOVA with Tukey's multiple comparisons test. **B** Illustration of spatial novelty Y-maze test setup, created with BioRender.com. **C** Representative heatmap of spatial novelty Y-maze during test phase in which the left arm was novel, in *Masp3*^{+/+} (left panel), *Masp3*^{+/-} (middle panel) and *Masp3*^{-/-} (right panel) mice. **D** Time spent and **E** distance run in the familiar (black dots) vs.

novel (red triangles) arm in spatial novelty Y-maze test. *Masp3*^{+/+}: n = 8 (familiar arm: 37.86 s ± 16.99 s, 244 cm ± 86.78 cm; novel arm: 62.54 s ± 18.70 s, 373.50 cm ± 124.238 cm); *Masp3*^{+/-}: n = 9 (familiar arm: 39.55 s ± 8.14 s, 222.49 cm ± 62.81 cm; novel arm: 63.96 s ± 8.51 s, 378.03 cm ± 60.80 cm); *Masp3*^{-/-}: n = 7 (familiar arm: 50.91 s ± 15.19 s, 282.08 cm ± 104.73 cm; novel arm: 49.13 s ± 13.48 s, 342.15 cm ± 91.69 cm); all male mice. Paired two-way ANOVA followed by Sidak's test for multiple comparison. Error bars represent standard deviation; ns not significant; *p < 0.05, **p < 0.01, ***p < 0.001, ****p < 0.0001. Source data are provided as a Source Data File.

complement activity. Similarly, shared components of the three complement activation pathways C2, C4b and C3 are lowly expressed, unlike in the periphery where C4b and C3 are among the most abundant serum proteins. The brain also uses tissue-specific regulation on transcript variants of the *Masp1* gene to moderate LP and AP activity, and, unlike in the periphery, the brain expresses high levels of the variant encoding *Map44* that inhibits LP. In addition, absence of local expression of the C5-encoding gene *Hc*, and the inability to access serum C5 due to the blood-brain barrier likely prevents MAC formation and subsequent lytic cell death in healthy brains. Moreover, the brain limits inflammation by preferentially expressing immunomodulatory C5a receptor *C5ar2* over *C5ar1*. Finally, canonical and brain-enriched complement regulators are abundantly expressed both by neurons and non-neuronal cells in the brain to provide an additional level of protection against complement attack.

Although a role of the CP activation in normal brain development^{3–6} and neurological diseases^{9–18} has been widely reported, little is known about the LP and the AP in the brain. Our transcriptional evidence suggests insufficient local expression to support LP activation, based on the subthreshold level of expression of LP serine proteases *Masp1* and *Masp2*, but abundant expression of LP inhibitor, *Map44*, throughout all ages tested. However, the role of LP in embryonic neural migration has been previously reported⁵⁵. It remains possible that trace levels of local *Masp1* and *Masp2* expression may be sufficient for LP activity in the brain. Alternatively, a peripheral source may activate brain LP, especially in embryonic and early postnatal brains when the blood-brain barrier is still immature. In addition, local production of LP could be activated in aging and disease conditions, for example, in traumatic brain injury^{56,57} and ischemic stroke in the brain⁵⁸.

On the other hand, our data indicated a presence of the AP in the developing brain, supported by the observation that all AP genes are locally expressed above the detection threshold. Spatially, *pan-Masp1* expression correlated with that of *Cfd*, a key AP gene and a direct downstream target of the *Masp3* isoform encoded by the *Masp1* gene that functions as AP activating serine protease. In addition, isoform-specific analyses revealed high expression of *Masp3*, rather than

Masp1, in embryonic and early postnatal brains. Transcriptional evidence by MERFISH showed that *Masp3* deficiency altered cortical distribution of subsets of vGlut1⁺ excitatory neurons in juvenile mice. Specifically, loss of *Masp3* caused reduction of excitatory neurons that expressed high levels of mature neuron markers such as *Slc17a7* and *Rbfox3* in the posterior cortex of neonatal mice. In parallel, adult *Masp3* deficient mice developed deficits in spatial working memory, consistent with the notion that *Masp3* may have a role in neural development. These phenotypes resemble the 3MC syndrome in human, a rare autosomal recessive disorder characterized by delayed development, abnormal facial cranial structure, short stature, and intellectual disabilities^{59,60}. In addition to mutations in LP genes (*MASPI*, *COLEC10* and *COLEC11*)⁶¹, it has been recently reported that homozygous loss-of-function mutations specifically affecting the *MASPI* transcript variant of the *MASPI* gene can also cause 3MC syndrome^{59,60}. In fact, 3MC causative mutations in the *MASPI* gene are either located in exons that are shared among all three transcript variants, or in exon 12, which is specific to the *MASPI* transcript^{59,61}, but no *MASPI* or *MAP44* isoform-specific mutations have been reported. This observation supports that, beyond the LP, the loss of *MASPI* may be a cause of the 3MC syndrome. However, although the most well-established molecular function of *Masp3* is the proteolytic activation of *Cfd* and thereby AP activation, it may act on other substrates outside of the complement cascade⁶². Further studies using *Cfb* or *Cfd*-deficient models are necessary to make the distinction.

While this study generated insights into the source of complement components, their regulation and potential function in the brain, these results should be interpreted with caution. Our analyses were primarily based on transcriptional data, yet RNA expression does not always align with protein abundance, due to factors such as post-transcriptional regulation, protein stability, secretion, or localization. Such a difference is particularly important to consider when studying the complement system, an enzymatic cascade primarily based on secreted proteins. Future development of reliable antibodies and functional assays suitable for the brain is essential to validate hypotheses generated based on RNA expression.

Methods

Mice

All animal experiments were performed in compliance with the Institutional Animal Care and Use Committee at Harvard Medical School and Boston Children's Hospital (protocol numbers IS00000111 and IS00002660), and with the guidelines of the Laboratory Animal Center at the NIH for the humane treatment of animals. Postnatal C57Bl/6J mice from p2 to p120 were used in this study (WT; The Jackson Laboratory, strain 000664). The strain was originally obtained from the Jackson Laboratory and then bred and maintained in-house. For embryonic C57Bl/6J mice, pregnant females with known gestational day was obtained from the Jackson Laboratory (strain 000664). The *Masp3* mutant mice were obtained from the Song lab at University of Pennsylvania, School of Medicine, and expanded in-house. Specifically, these mice are on a C57Bl/6J background, and exon 12 of the *Masp1* gene was deleted using CRISPR/Cas9⁵⁴. 5-day-old *Masp3* mutant mice were used for MERFISH and RNAscope, adult *Masp3* mutant mice (10–14-week-old) were used for serum collection for hemolytic assay and behavioral tests. All mice were maintained at the AAALAC accredited animal facility at Harvard Medical School, at ambient temperature between 20 and 22 °C and 40% to 60% humidity with a 12-h light-dark cycle and fed with standard chow diet and water ad libitum.

MERFISH library target gene selection

We selected a panel of 249 genes composed of seven major categories: (1) complement related genes (a total of 51 genes, including 26 complement components, 13 known and putative complement receptors in the brain, and 12 complement regulators^{1,2,35,41–43,50,51,63,64}; (2) brain cell type markers (2–3 well-established markers per brain cell type)^{34,65}; (3) brain region markers selected based on empirical data and ABA reference ISH results; (4) genes related to neuronal function (including a comprehensive list of neurotransmitter synthesis, transports and receptors) and homeostasis selected based on empirical data; (5) astrocyte function related to neurodevelopment and disease conditions^{66–68}; (6) microglia in neurodevelopment and disease conditions^{69–71}; (7) other genes implicated in neurodevelopmental disorders. These genes are listed in Table S1.

MERFISH probe sequence design and probe library construction

MERFISH probe sequences were designed using a previously established protocol^{19–21}. Each target gene in our library was assigned a unique 24-bit binary barcode with Hamming distance 4, and Hamming weight 4. The Ensembl Genome Reference Consortium Mouse Build 38 (mm10) was used as the reference transcript sequences. When a gene of interest has multiple isoforms, the predominantly expressed isoform was selected as the reference sequence. If multiple isoforms were expressed at a comparable level, probes were not penalized for targeting multiple isoforms. 80 distinct probes were designed for each target gene, though a few genes too short to support this number of probes had fewer. Each probe contains one 30-nt targeting sequence complementary to the target gene that has minimal homology to other genes. Overlap of the 30-nt complementary region between probes for the same target gene was allowed. To each targeting sequence, three 20-nt readout regions were concatenated, the sequence of which is complementary to the readout probe sequence whose associated bit in the barcode assigned to that gene contained a “1”. The probe sequences are deposited on Data Dryad (<https://doi.org/10.5061/dryad.cnphqcbq>). The template oligopool library was custom synthesized by Twist Biosciences and amplified to generate the final probe library for hybridization following a published protocol^{19–21}.

MERFISH sample preparation, imaging and decoding of raw image data

Samples for MERFISH were prepared as previously described^{19–21}. Briefly, mice were euthanized with isoflurane overdose. Brains were

quickly dissected and immediately frozen on dry ice and stored at -80 °C until sectioning. Sagittal slices of 14-μm thickness were collected at 960 ± 80 μm from the midline in E18.5 mice; 960 ± 80 μm, and 2040 ± 80 μm from the midline in p5 mice, 1000 ± 100 μm, and 2450 ± 100 μm from the midline in p60 mice, and 1000 ± 100 μm from the midline in p120 mice. Brain slices were collected on poly-D-lysine-coated silanized glass coverslips covered with orange fiducial beads that were prepared as previously described²¹. Brain sections were allowed to air dry, then fixed in 4% paraformaldehyde (PFA) for 10 min at room temperature, and washed three times with RNase-free PBS. Fixed brain slices were stored in 70% ethanol for at least 16 h (and up to 3 days) before hybridization. Encoding probe hybridization was performed at 37 °C for 48 h in a humidified chamber inside a covered petri dish as previously described²¹. Samples were then washed, embedded in polyacrylamide gel, and treated with proteinase K as previously described²¹. Fully prepared samples were stored in RNase-free 2X SSC at 4 °C for less than 3 days before imaging. Images were collected on a custom microscope and fluidic system as described previously⁷². Z stacks of 10-μm thickness at 1-μm step size were taken for each field of view. 12 cycles of two-color readout probe hybridization, imaging, fluorophore cleavage, and wash were performed to measure signals for the 24-bit barcode scheme. The total imaging time for a full sagittal section was ~36–40 h. To ensure optimal signal, buffers and readout probe solutions were replaced with fresh preparations after six cycles of imaging. Raw MERFISH imaging data were decoded using a previously established pipeline^{19–21}. In the pipeline, cells were segmented relying on nuclei and total cytoplasmic RNA signals, using a watershed-based algorithm as previously described^{19–21}. Only counts found within the cell body were used in downstream analyses.

MERFISH data analyses

MERFISH decoding was performed with previously published code^{19,20} available on Github at https://github.com/ZhuangLab/MERFISH_analysis. All downstream MERFISH analyses were performed with custom code in Python 3.7.4 (deposited on Data Dryad, <https://doi.org/10.5061/dryad.cnphqcbq>). Features with a volume above 100 μm³ were considered cells, those below the volume threshold were removed, as well as cells with zero total RNA counts. Data were normalized by cell volume and then scaled to bring the total number of RNA counts per cell to 250. RNA counts were then log transformed for cell type clustering with the Scanpy package⁷³ following the standard workflow. To correct for batch effect, the Harmony algorithm⁷⁴ was applied after principal component analysis (PCA), and the corrected PCs were used for clustering. Primary clustering was performed using the Leiden algorithm⁷⁵ with kNN = 30 and resolution = 1. Neuronal cell types identified from primary clustering were regrouped into inhibitory neurons, vGlut1⁺ neurons and vGlut2⁺ excitatory neurons. Secondary clustering was then performed for each primary cell type with individually kNN and resolution adjusted to avoid over-clustering.

For experiments performed on p5 *Masp3*^{+/+} and *Masp3*^{-/-} brains, to minimize batch effect while preserving biological differences, each MERFISH run was composed of one *Masp3*^{+/+} and one *Masp3*^{-/-} sample. A total of 3 MERFISH datasets were then integrated, and batch effects were removed with Harmony⁷⁴ prior to cell type clustering.

Brain region assignment

For brain region identification, the spatial distribution of each refined cluster was plotted and compared with Allen Brain Atlas. Cell types that showed spatial specificity were used as reference clusters for brain region assignment. For each individual cell, the identity of its top 30 spatially nearest neighbor cells was calculated using the NearestNeighbors function from sklearn.neighbors python package. The cell was assigned to the brain region based on the most frequently found reference cell within its vicinity. The cell was assigned “NA” if a consensus brain region reference cell could not be identified.

Aggregated complement expression score

Average expression of each complement gene was calculated by brain region. Aggregated expression score per brain region was computed as the geometric mean of the average expression of complement components involved in each pathway. For plotting purposes, all cells within the given brain region were assigned the aggregated score calculated for that region.

RNA expression analysis by ddPCR and qRT-PCR

Mouse anterior cortices were dissected after transcardiac perfusion with 20 ml ice-cold RNase-free PBS. Brain tissue samples were lysed in the presence of TRIzol reagent (Ambion 15-596-018) with TissueLyser homogenizer (Qiagen 85600). RNA was isolated using phenol-chloroform extraction followed by purification with Zymo Direct-zol RNA Miniprep Kit (Zymo Research R2052). Genomic DNA removal and cDNA synthesis were performed with iScript gDNA clear cDNA synthesis kit (Bio-Rad 1725035) by following manufacturer's instructions. ddPCR reactions were run with QX200™ ddPCR™ EvaGreen Supermix (Bio-Rad 186-4034). Each 20 μ l reaction mix contains 10 μ l EvaGreen Supermix, 0.5 μ l primer mix at 5 μ M each, and 9.5 μ l of cDNA. Droplets containing the reaction mixture was generated by the Bio-Rad microfluidic droplet generator, PCR amplified using the following cycle conditions: 95 °C for 3 min, 40 cycles of 95 °C for 20 s, 60 °C for 20 s and 72 °C for 30 s, and then read with the Bio-Rad QX100 droplet reader. Data were analyzed using Bio-Rad QuantaSoft software v.1.7.4.0917. qRT-PCR was performed using iTaq™ universal SYBR® Green supermix system (Bio-Rad 1725124) and run on the Bio-Rad CFX96 real-time system with the same cycle conditions as in ddPCR. Signal was read at the end of each 60 °C incubation period. *Hprt1* was used as reference gene in both ddPCR and qRT-PCR. Primers for ddPCR and qRT-PCR were designed using the PrimerBank primer designing tool developed by Harvard Medical School/Massachusetts General Hospital. *Hprt1* (fwd: GCGTCGTGATTAGCGATGATG; rev: CTCGAGCAAGTCTTCAGTCC); *Masp1* (fwd: AGTGCTCAAGAGAAG CCTGC; rev: AGCAGCTGTCAAAACCCAGT)³⁶; *Masp3* (fwd: AGTGCTC AAGAGAACGCTGC; rev: ACCCTCGATGTCTTCCAC)³⁶; *Map44* (fwd: CAAAGACCAAGTGTCTCGTCA; rev: CTTCTCCAATTGATCTCGC)³⁶.

RNAscope™ in situ hybridization

RNAscope™ in situ hybridization was performed on fresh frozen brain sections of 14 μ m thickness. The RNAscope™ Fluorescent Multiplex Assay kit (ACDBio, 323130) was used. Samples were prepared following the manufacturer's instructions. Probes: *Mm-Masp1*, channel 1 (isoform non-specific, ACDBio 525851-C1); *Mm-Masp1-O1*, channel 1 (*Masp3*-specific customized probe for NM_001359083.1, ACDBio 1176541-C1); *Mm-Masp1-O2*, channel 1 (*Masp1*-specific customized probe for NM_008555.3, ACDBio 1193891-C1); *Mm-Masp1-O4*, channel 1 (*Map44*-specific customized probe for XM_006521829.5, ACDBio 201741-C1); *Slc17a7* (ACDBio, 416631-C1). Images were obtained using an Olympus Fluoview FV1000 confocal microscope with 40 \times magnification objectives. *Slc17a7* density in superficial cortical layers was quantified with ImageJ (version 1.54p) and normalized to DAPI nuclei area in the region of interest.

Rabbit red blood cell hemolytic assay for alternative complement activation

Rabbit RBC hemolytic assay was performed as previously described⁵⁴. Briefly, rabbit red blood cell (Complement technology, B300) was washed in GVB° (Ca²⁺ and Mg²⁺ free, Complement technology, B103) buffer and diluted to 10⁹/ml in the same GVB° buffer. Mouse EDTA plasma was diluted to 40% in GVB-Mg²⁺EGTA (5 mM) buffer. Diluted plasma was incubated with 10 μ l of diluted rabbit RBC in a final volume of 50 μ l and incubated at 37 °C for 30 min in a water bath with mixing. For complete hemolysis control, 10 μ l diluted rabbit RBC was added to 40 μ l of H₂O. 10 mM EDTA was added at the end of incubation to stop

the reaction. Cells were centrifuged at 1000 x g for 5 min at 4 °C. OD 405 nm was read on the supernatant. Percent hemolysis was calculated as sample OD405nm divided by OD405 of RBC lysis in H₂O.

Spatial novelty Y maze test

Mice were allowed to acclimate for at least 30 min prior to starting the test. The experiment was run in a clear, Y-shaped 3-arm maze with a 120° angle between the arms. Each mouse was run twice in the Y-Maze, first for a 3 min habituation phase then for a 3 min test phase, with a delay of 2 min from the end habituation phase and the beginning of test phase. The testing arena was cleaned after each trial. For each trial, the mouse was always introduced in the same arm, denoted as "starting arm". For habituation phase, one arm was blocked off, which was randomized and balanced for genotypes. For the test phase, the blockade was removed, the mouse was re-introduced and allowed to freely explore the entire testing arena. All trials were video recorded and analyzed using EthoVision XT 17 software (Noldus). The time spent and distance run in the familiar and the novel arms were compared.

Light-dark box test

Mice were allowed to acclimate for at least 30 min prior to starting the test. The experiment was run in an ENV-520 open-field arena (Med Associates) that was equally divided into two chambers with a small opening in between. One chamber was under direct illumination (650 lux), and the other chamber was protected from light with a black opaque insertion. The test mouse was introduced to the center of the light chamber and was allowed to run freely in both chambers for 10 min. Its movement was tracked with infrared beams, and all data were recorded and analyzed with the Activity Monitor software from Med Associates. The percentage of time spent and distance run in the light chamber are reported.

Open field test for locomotion

Mice were allowed to acclimate for at least 30 min prior to starting the test. The experiment was performed in a clear 27 \times 27 \times 20 cm³ Plexiglas chamber from Med Associates. The test mouse was allowed to run freely in the test arena for 1 h and tracked with infrared tracking system. Data were recorded and analyzed with the Activity Monitor software from Med associates. The total distance traveled (cm) was reported for general locomotor activity.

Rotarod test

Mice were allowed to acclimate for at least 30 min prior to starting the test. The experiment was performed on a rotarod apparatus (Stoelting; Ugo Basile Apparatus) consists a texturized plastic roller flanked by large round dividers to isolate test mice. Mice are tested in groups of up to five mice. A habituation run with performed by letting the mice run on the rod rotating at 4 rpm for 5 min. During this step, mice were replaced back to run if they drop from the rotating rod. Following habituation, mice were reintroduced to the rotarod apparatus and tested with accelerating rod rotation speed (4–40 rpm in 3 min, maintained at 40 rpm for a total of 5 min). Mice were tested three times, and the average latency to fall across three trials was reported. Mice were allowed to rest for at least 20 min between trials.

Tail suspension test

Mice were allowed to acclimate for at least 30 min prior to starting the test. In this experiment, a 4 cm plastic thin tube was introduced to the test mouse's tail as a climb stopper. A five-centimeter scotch tape was adhered and folded in half around the tip of the test mouse's tail. The test mouse was hooked to the test arena and suspended upside down for 10 min, without being able to touch the bottom of the test arena. Its movement was recorded, tracked and analyzed with the EthoVision XT 17 software (Noldus). The total immobile time was reported.

Forced swim test

Mice were allowed to acclimate for at least 30 min prior to starting the test. This experiment was performed in 2000 ml Pyrex beakers with a diameter of approximately 12 cm, filled with $25 \pm 1^\circ\text{C}$ water to the 1400 ml mark. The test mouse was weighed before the start of the test and each trial duration was 6 min. The test mouse's movement was recorded, tracked and analyzed with the EthoVision XT 17 software (Noldus) and the total immobile time was reported.

Statistics

Statistical analyses were performed in Python and GraphPad Prism 8.3.0. All data in dot plots were presented as mean \pm standard deviation. One-way or two-way ANOVA was applied for multiple group comparisons. Pair-wise comparisons were performed using appropriate multiple comparison tests. Detailed statistical methods used were indicated in the figure legend. Exact *p* values are included in Table S5.

Reporting summary

Further information on research design is available in the Nature Portfolio Reporting Summary linked to this article.

Data availability

Source data are provided with this paper. MERFISH probe sequences, decoded raw data in this study, have been deposited on Data Dryad (<https://doi.org/10.5061/dryad.cnp5hqcq>). We also constructed an interactive online platform (https://moffitlab.github.io/visualization/2024_Complement_Brain/index.html) to facilitate spatial data visualization, and to provide additional cell type, brain region and age-dependent differential expression analyses. Source data are provided with this paper.

Code availability

Code for MERFISH decoding was published previously^{19,20} and is available on Github at https://github.com/ZhuangLab/MERFISH_analysis. Code for additional analyses performed in this study has been deposited on Data Dryad (<https://doi.org/10.5061/dryad.cnp5hqcq>).

References

- Carroll, M. C. The complement system in regulation of adaptive immunity. *Nat. Immunol.* **5**, 981–986 (2004).
- Ricklin, D., Hajishengallis, G., Yang, K. & Lambris, J. D. Complement: a key system for immune surveillance and homeostasis. *Nat. Immunol.* **11**, 785–797 (2010).
- Presumey, J., Bialas, A. R. & Carroll, M. C. Complement system in neural synapse elimination in development and disease. *Adv. Immunol.* **135**, 53–79 (2017).
- Schafer, D. P. et al. Microglia sculpt postnatal neural circuits in an activity and complement-dependent manner. *Neuron* **74**, 691–705 (2012).
- Stephan, A. H., Barres, B. A. & Stevens, B. The complement system: an unexpected role in synaptic pruning during development and disease. *Annu Rev. Neurosci.* **35**, 369–389 (2012).
- Stevens, B. et al. The classical complement cascade mediates CNS synapse elimination. *Cell* **131**, 1164–1178 (2007).
- Druart, M. et al. Elevated expression of complement C4 in the mouse prefrontal cortex causes schizophrenia-associated phenotypes. *Mol. Psychiatry* **26**, 3489–3501 (2021).
- Schizophrenia Working Group of the Psychiatric Genomics Consortium Biological insights from 108 schizophrenia-associated genetic loci. *Nature* **511**, 421–427 (2014).
- Sekar, A. et al. Schizophrenia risk from complex variation of complement component 4. *Nature* **530**, 177–183 (2016).
- Yilmaz, M. et al. Overexpression of schizophrenia susceptibility factor human complement C4A promotes excessive synaptic loss and behavioral changes in mice. *Nat. Neurosci.* **24**, 214–224 (2021).
- Dalakas, M. C., Alexopoulos, H. & Spaeth, P. J. Complement in neurological disorders and emerging complement-targeted therapeutics. *Nat. Rev. Neurol.* **16**, 601–617 (2020).
- Hong, S. et al. Complement and microglia mediate early synapse loss in Alzheimer's mouse models. *Science* **352**, 712–716 (2016).
- Kjaeldgaard, A. L. et al. Amyotrophic lateral sclerosis: the complement and inflammatory hypothesis. *Mol. Immunol.* **102**, 14–25 (2018).
- Krance, S. H. et al. The complement cascade in Alzheimer's disease: a systematic review and meta-analysis. *Mol. Psychiatry* **26**, 5532–5541 (2021).
- Shi, Q. et al. Complement C3 deficiency protects against neurodegeneration in aged plaque-rich APP/PS1 mice. *Sci. Transl. Med.* **9**, <https://doi.org/10.1126/scitranslmed.aaf6295> (2017).
- Watkins, L. M. et al. Complement is activated in progressive multiple sclerosis cortical grey matter lesions. *J. Neuroinflammation* **13**, 161 (2016).
- Werneburg, S. et al. Targeted complement inhibition at synapses prevents microglial synaptic engulfment and synapse loss in demyelinating disease. *Immunity* **52**, 167–182.e167 (2020).
- Wilton, D. K. et al. Microglia and complement mediate early corticostratal synapse loss and cognitive dysfunction in Huntington's disease. *Nat. Med.* **29**, 2866–2884 (2023).
- Chen, K. H., Boettiger, A. N., Moffitt, J. R., Wang, S. & Zhuang, X. R. N. A. imaging. Spatially resolved, highly multiplexed RNA profiling in single cells. *Science* **348**, aaa6090 (2015).
- Moffitt, J. R. et al. Molecular, spatial, and functional single-cell profiling of the hypothalamic preoptic region. *Science* **362**, <https://doi.org/10.1126/science.aau5324> (2018).
- Moffitt, J. R. et al. High-throughput single-cell gene-expression profiling with multiplexed error-robust fluorescence in situ hybridization. *Proc. Natl. Acad. Sci. USA* **113**, 11046–11051 (2016).
- Allen, W. E., Blosser, T. R., Sullivan, Z. A., Dulac, C. & Zhuang, X. Molecular and spatial signatures of mouse brain aging at single-cell resolution. *Cell* **186**, 194–208.e118 (2023).
- Fang, R. et al. Conservation and divergence of cortical cell organization in human and mouse revealed by MERFISH. *Science* **377**, 56–62 (2022).
- Zhang, M. et al. Spatially resolved cell atlas of the mouse primary motor cortex by MERFISH. *Nature* **598**, 137–143 (2021).
- Zhang, M. et al. Molecularly defined and spatially resolved cell atlas of the whole mouse brain. *Nature* **624**, 343–354 (2023).
- Shi, H. et al. Spatial atlas of the mouse central nervous system at molecular resolution. *Nature* **622**, 552–561 (2023).
- Yao, Z. et al. A high-resolution transcriptomic and spatial atlas of cell types in the whole mouse brain. *Nature* **624**, 317–332 (2023).
- Stephan, A. H. et al. A dramatic increase of C1q protein in the CNS during normal aging. *J. Neurosci.* **33**, 13460–13474 (2013).
- Murata, Y. & Colonnese, M. T. Thalamic inhibitory circuits and network activity development. *Brain Res.* **1706**, 13–23 (2019).
- Pham, T. & Haas, J. S. Electrical synapses between inhibitory neurons shape the responses of principal neurons to transient inputs in the thalamus: a modeling study. *Sci. Rep.* **8**, 7763 (2018).
- Cox, C. L., Huguenard, J. R. & Prince, D. A. Nucleus reticularis neurons mediate diverse inhibitory effects in thalamus. *Proc. Natl. Acad. Sci. USA* **94**, 8854–8859 (1997).
- Fonseca, M. I. et al. Cell-specific deletion of C1qa identifies microglia as the dominant source of C1q in mouse brain. *J. Neuroinflammation* **14**, 48 (2017).
- Herring, C. A. et al. Human prefrontal cortex gene regulatory dynamics from gestation to adulthood at single-cell resolution. *Cell* **185**, 4428–4447.e4428 (2022).

34. Zeisel, A. et al. Molecular architecture of the mouse nervous system. *Cell* **174**, 999–1014.e1022 (2018).

35. Hourcade, D. E. The role of properdin in the assembly of the alternative pathway C3 convertases of complement. *J. Biol. Chem.* **281**, 2128–2132 (2006).

36. Hayashi, M. et al. Cutting Edge: role of MASP-3 in the physiological activation of factor d of the alternative complement pathway. *J. Immunol.* **203**, 1411–1416 (2019).

37. Xie, C. B., Jane-Wit, D. & Pober, J. S. Complement membrane attack complex: new roles, mechanisms of action, and therapeutic targets. *Am. J. Pathol.* **190**, 1138–1150 (2020).

38. Zelek, W. M., Bevan, R. J. & Morgan, B. P. Targeting terminal pathway reduces brain complement activation, amyloid load and synapse loss, and improves cognition in a mouse model of dementia. *Brain Behav. Immun.* **118**, 355–363 (2024).

39. Carpanini, S. M. et al. Terminal complement pathway activation drives synaptic loss in Alzheimer’s disease models. *Acta Neuropathol. Commun.* **10**, 99 (2022).

40. Li, X. X., Lee, J. D., Kemper, C. & Woodruff, T. M. The Complement receptor C5aR2: a powerful modulator of innate and adaptive immunity. *J. Immunol.* **202**, 3339–3348 (2019).

41. Kovacs, R. A. et al. Identification of neuronal pentraxins as synaptic binding partners of C1q and the involvement of NP1 in synaptic pruning in adult mice. *Front. Immunol.* **11**, 599771 (2020).

42. Zhou, J. et al. The neuronal pentraxin Nptx2 regulates complement activity and restrains microglia-mediated synapse loss in neurodegeneration. *Sci. Transl. Med.* **15**, eadfo141 (2023).

43. Battin, C. et al. Neuropilin-1 acts as a receptor for complement split products. *Front. Immunol.* **10**, 2209 (2019).

44. Giger, R. J. et al. Neuropilin-2 is a receptor for semaphorin IV: insight into the structural basis of receptor function and specificity. *Neuron* **21**, 1079–1092 (1998).

45. Gu, C. et al. Neuropilin-1 conveys semaphorin and VEGF signaling during neural and cardiovascular development. *Dev. Cell* **5**, 45–57 (2003).

46. Gorelik, A., Sapir, T., Woodruff, T. M. & Reiner, O. Serping1/C1 inhibitor affects cortical development in a cell autonomous and non-cell autonomous manner. *Front. Cell Neurosci.* **11**, 169 (2017).

47. Kraus, D. M. et al. CSMD1 is a novel multiple-domain complement regulatory protein highly expressed in the central nervous system and epithelial tissues. *J. Immunol.* **176**, 4419–4430 (2006).

48. Baum, M. L. et al. CSMD1 regulates brain complement activity and circuit development. *Brain Behav. Immun.* **119**, 317–332 (2024).

49. Byrne, R. A. J. et al. The schizophrenia-associated gene CSMD1 encodes a complement classical pathway inhibitor predominantly expressed by astrocytes and at synapses in mice and humans. *Brain Behav. Immun.* **127**, 287–302 (2025).

50. Sheehan, M., Morris, C. A., Pussell, B. A. & Charlesworth, J. A. Complement inhibition by human vitronectin involves non-heparin binding domains. *Clin. Exp. Immunol.* **101**, 136–141 (1995).

51. Tschopp, J., Chonn, A., Hertig, S. & French, L. E. Clusterin, the human apolipoprotein and complement inhibitor, binds to complement C7, C8 beta, and the b domain of C9. *J. Immunol.* **151**, 2159–2165 (1993).

52. Rollins, S. A. & Sims, P. J. The complement-inhibitory activity of CD59 resides in its capacity to block incorporation of C9 into membrane C5b-9. *J. Immunol.* **144**, 3478–3483 (1990).

53. Degn, S. E. et al. Biological variations of MASP-3 and MAp44, two splice products of the MASP1 gene involved in regulation of the complement system. *J. Immunol. Methods* **361**, 37–50 (2010).

54. Gullipalli, D. et al. MASP3 deficiency in mice reduces but does not abrogate alternative pathway complement activity due to intrinsic profactor D activity. *J. Immunol.* **210**, 1543–1551 (2023).

55. Gorelik, A. et al. Developmental activities of the complement pathway in migrating neurons. *Nat. Commun.* **8**, 15096 (2017).

56. De Blasio, D. et al. Pharmacological inhibition of mannose-binding lectin ameliorates neurobehavioral dysfunction following experimental traumatic brain injury. *J. Cereb. Blood Flow. Metab.* **37**, 938–950 (2017).

57. Mercurio, D. et al. Targeted deletions of complement lectin pathway genes improve outcome in traumatic brain injury, with MASP-2 playing a major role. *Acta Neuropathol. Commun.* **8**, 174 (2020).

58. Fumagalli, S. & De Simoni, M. G. Lectin Complement pathway and its bloody interactions in brain ischemia. *Stroke* **47**, 3067–3073 (2016).

59. Atik, T. et al. Novel MASP1 mutations are associated with an expanded phenotype in 3MC1 syndrome. *Orphanet J. Rare Dis.* **10**, 128 (2015).

60. Pihl, R. et al. Analysis of factor D isoforms in Malpuech-Michels-Mingarelli-Carnevale patients highlights the role of masp-3 as a maturase in the alternative pathway of complement. *J. Immunol.*, <https://doi.org/10.4049/jimmunol.1700518> (2017).

61. Gajek, G., Swierzko, A. S. & Cedzynski, M. Association of polymorphisms of MASP1/3, COLEC10, and COLEC11 genes with 3MC syndrome. *Int. J. Mol. Sci.* **21**, <https://doi.org/10.3390/ijms21155483> (2020).

62. Cortesio, C. L. & Jiang, W. Mannan-binding lectin-associated serine protease 3 cleaves synthetic peptides and insulin-like growth factor-binding protein 5. *Arch. Biochem. Biophys.* **449**, 164–170 (2006).

63. Krych, M., Atkinson, J. P. & Holers, V. M. Complement receptors. *Curr. Opin. Immunol.* **4**, 8–13 (1992).

64. Zipfel, P. F. & Skerka, C. Complement regulators and inhibitory proteins. *Nat. Rev. Immunol.* **9**, 729–740 (2009).

65. Codeluppi, S. et al. Spatial organization of the somatosensory cortex revealed by osmFISH. *Nat. Methods* **15**, 932–935 (2018).

66. Chung, W. S. et al. Astrocytes mediate synapse elimination through MEGF10 and MERTK pathways. *Nature* **504**, 394–400 (2013).

67. Clarke, L. E. & Barres, B. A. Emerging roles of astrocytes in neural circuit development. *Nat. Rev. Neurosci.* **14**, 311–321 (2013).

68. Zamanian, J. L. et al. Genomic analysis of reactive astrogliosis. *J. Neurosci.* **32**, 6391–6410 (2012).

69. Hammond, T. R. et al. Single-cell RNA sequencing of microglia throughout the mouse lifespan and in the injured brain reveals complex cell state changes. *Immunity* **50**, 253–271.e256 (2019).

70. Keren-Shaul, H. et al. A unique microglia type associated with restricting development of Alzheimer’s disease. *Cell* **169**, 1276–1290.e1217 (2017).

71. Lehrman, E. K. et al. CD47 protects synapses from excess microglia-mediated pruning during development. *Neuron* **100**, 120–134.e126 (2018).

72. Cadinu, P. et al. Charting the cellular biogeography in colitis reveals fibroblast trajectories and coordinated spatial remodeling. *Cell* **187**, 2010–2028.e2030 (2024).

73. Wolf, F. A., Angerer, P. & Theis, F. J. SCANPY: large-scale single-cell gene expression data analysis. *Genome Biol.* **19**, 15 (2018).

74. Korsunsky, I. et al. Fast, sensitive and accurate integration of single-cell data with Harmony. *Nat. Methods* **16**, 1289–1296 (2019).

75. Traag, V. A., Waltman, L. & van Eck, N. J. From Louvain to Leiden: guaranteeing well-connected communities. *Sci. Rep.* **9**, 5233 (2019).

Acknowledgements

This work was supported by NIH grants NIMH P50MH112491 (M.C.C.), NIGMS R01GM143277 (J.R.M.) and the Brain and Behavior Research Foundation young investigator grant 32430 (Y.Z.). Additionally, we thank

Drs. Aritra Bhattacherjee and Chao Zhang for discussion and advice. We thank Elisabeth Elicot and Diana Pascual for administrative support and mouse colony management.

Author contributions

M.C.C. conceived the project; M.C.C., J.R.M. supervised the project; Y.Z., B.C., J.R.M., M.C.C. designed the experiments; Y.Z. designed, performed and analyzed MERFISH experiments; B.W. constructed the MERFISH instrument, performed user training, and prepared essential non-commercial reagents; T.L., S.C., L.G. constructed the MERFISH data visualization website; Y.Z. performed qRT-PCR, ddPCR, RNAscope; A.R. performed rabbit red blood cell hemolytic assay; Y.Z., Y.G. performed mouse behavior tests; F.B.L performed RNAscope and generated summary figure; M.M. performed mouse genotyping; T.M., M.G., W.S. generated the *Masp3*^{-/-} mouse model; Y.Z., J.R.M., M.C.C. wrote the manuscript.

Competing interests

J.R.M. is a co-founder of, stakeholder in, and advisor for Vizgen, Inc. J.R.M. is an inventor on published patents (US62/050,636; US62/031,062; and US62/419,033) that describe the MERFISH technology used in this work. These patents were applied for on behalf of J.R.M. by Harvard University. J.R.M.'s interests were reviewed and are managed by Boston Children's Hospital in accordance with its conflict-of-interest policies. Other authors declare no conflict of interest.

Additional information

Supplementary information The online version contains supplementary material available at <https://doi.org/10.1038/s41467-025-66048-5>.

Correspondence and requests for materials should be addressed to Jeffrey R. Moffitt or Michael C. Carroll.

Peer review information *Nature Communications* thanks the anonymous reviewers for their contribution to the peer review of this work. A peer review file is available.

Reprints and permissions information is available at <http://www.nature.com/reprints>

Publisher's note Springer Nature remains neutral with regard to jurisdictional claims in published maps and institutional affiliations.

Open Access This article is licensed under a Creative Commons Attribution-NonCommercial-NoDerivatives 4.0 International License, which permits any non-commercial use, sharing, distribution and reproduction in any medium or format, as long as you give appropriate credit to the original author(s) and the source, provide a link to the Creative Commons licence, and indicate if you modified the licensed material. You do not have permission under this licence to share adapted material derived from this article or parts of it. The images or other third party material in this article are included in the article's Creative Commons licence, unless indicated otherwise in a credit line to the material. If material is not included in the article's Creative Commons licence and your intended use is not permitted by statutory regulation or exceeds the permitted use, you will need to obtain permission directly from the copyright holder. To view a copy of this licence, visit <http://creativecommons.org/licenses/by-nc-nd/4.0/>.

© The Author(s) 2025